Molecular nature of the $a_1(1260)$ axial-vector meson

Samson Clymton[1, *] and Hyun-Chul Kim[1, 2, †]

[1] *Department of Physics, Inha University, Incheon 22212, Republic of Korea*

[2] *School of Physics, Korea Institute for Advanced Study (KIAS), Seoul 02455, Republic of Korea*

We investigate $\pi\rho$ scattering based on the coupled-channel formalism with the $\pi\rho$ and $K\bar{K}^*$ ($\bar{K}K^*$) channels included. We construct the kernel amplitudes by using the meson-exchange model and compute the coupled integral equation for $\pi\rho$ scattering. By performing the partial-wave expansion, we show explicitly that the $a_1(1260)$ meson is dynamically generated by the coupled-channel formalism. The a_1 meson only appears by including the $K\bar{K}^*$ ($\bar{K}K^*$) channel. We obtain the pole position of the a_1 meson as $\sqrt{s_R} = (1170.7 - i173.0)$ MeV. We conclude that the a_1 meson can be interpreted as a kaon and vector kaon molecular state.

arXiv:2208.04124v2 [hep-ph] 8 Nov 2022

I. INTRODUCTION

The $a_1(1260)$ meson is the first axial-vector meson. If chiral symmetry SU(2) $\otimes$ SU(2) is unbroken, then the ρ and a_1 mesons form a chiral doublet [1, 2] as the π and σ ($f_0(500)$) do. The existence of the a_1 meson has been well established since the ACCMOR Collaboration [3] confirmed it in partial wave analyses of the $\pi^-\pi^-\pi^+$ system. However, the values of its mass and width do not reach an experimental consensus. For example, the ARGUS Collaboration at DESY [4] found the mass of the a_1 meson to be $m_{a_1} = (1\,046 \pm 11)$ MeV and its width to be $\Gamma_{a_1} = (521 \pm 27)$ MeV in the decay $\tau \to \pi^-\pi^-\pi^+\nu_\tau$ whereas the CLEO Collaboration announced a rather large values $m_{a_1} = (1\,331 \pm 10 \pm 3)$ MeV and $\Gamma_{a_1} = (814 \pm 36 \pm 13)$ MeV in the decay $\tau \to \pi^-\pi^0\pi^0\nu_\tau$ [5]. Recently, the LHCb Collaboration measured $m_{a_1} = (1\,195.050 \pm 1.045 \pm 6.333)$ MeV and $\Gamma_{a_1} = (422.013 \pm 2.096 \pm 12.723)$ MeV in $D^0 \to K^\mp\pi^\pm\pi^\pm\pi^\mp$ decays [6]. Moreover, one should keep in mind that there is an inevitable model dependence in analyzing the experimental data. The Particle Data Group (PDG) estimates the average values of the a_1 mass and width as $m_{a_1} = (1\,230 \pm 40)$ MeV and $\Gamma_{a_1} = (420 \pm 35)$ MeV.

Since the a_1 meson has quantum numbers as $J^{PC} = 1^{++}$, it can be constructed as $q\bar{q}$ ($^3\mathrm{P}_1$) state. It is an isovector meson with negative G parity. Dankowych et al. [7] carried out the isobar-model partial-wave analysis of high statistics data on $\pi^- p \to \pi^+\pi^-\pi^0 n$ from the Argonne National Laboratory zero-gradient synchrotron. They extracted the partial-wave cross section of $\pi\rho$ scattering in S and D waves. The a_1 resonance was observed in the S-wave cross section with the broad width, which reaches the kaon and vector kaon ($\bar{K}K^*$) threshold. It was even seen that the a_1 meson decays into $\bar{K}$ and K^* [5, 8, 9]. It implies that the a_1 meson may be strongly coupled to the K and K^*. Thus, the a_1 meson may contain the tetraquark component, or it can even be interpreted as the molecular state [10–13]. A similar situation can be found in the case of the scalar-isovector meson $a_0(980)$, which is often interpreted either as a tetraquark state or as a resonance appearing from the $\pi\eta$ and $K\bar{K}$ coupled channels [14–17]. The scalar mesons $f_0(500)$ and $f_0(980)$ meson are also considered as the tetraquark or molecular states [16, 18–22]. In particular, the $f_0(980)$ is just below the $K\bar{K}$ threshold, it can be regarded as a $K\bar{K}$ molecular state [19, 23].

Janssen et al. [24] constructed the meson-exchange model for $\pi\rho$ scattering with the effective Lagrangian, including the a_1 meson explicitly. In the present work, we will extend the work of Ref. [24] by considering the coupled-channel formalism. We add the $K\bar{K}^*$ ($\bar{K}K^*$) channel to the $\pi\rho$ channel but exclude the a_1 meson. We will show how the $K\bar{K}^*$ ($\bar{K}K^*$) channel generates dynamically the a_1 meson and describe successfully the S-wave cross section. We first formulate the kernel amplitude based on the meson-exchange model. We treat the vector meson based on the hidden local gauge symmetry [25, 26]. This has a certain merit that the coupling constants are constrained. Then we solve the coupled integral equation for $\pi\rho$ scattering. The results for the S-wave cross section clearly reveals the a_1 meson with a broad width. We find the pole position in the second Riemann sheet as $\sqrt{s_R} = (1\,170.7 - i173.0)$ MeV.

* E-mail: sclymton@inha.edu

† E-mail: hchkim@inha.ac.kr

II. GENERAL FORMALISM

We start from the definition of the scattering amplitude expressed as

$$\mathcal{S}_{fi} = \delta_{fi} - i(2\pi)^4\delta^4(P_f - P_i)\mathcal{T}_{fi}, \tag{1}$$

where P_f and P_i denote the total four-momenta of the final and initial state. The formal transition amplitude $\mathcal{T}_{fi}$ is obtained from the Bethe-Salpeter (BS) equation with the coupled-channel formalism employed:

$$\mathcal{T}_{fi}(p', p; s) = \mathcal{V}_{fi}(p', p; s) + \frac{1}{(2\pi)^4}\int d^4q \mathcal{V}_{fk}(p', q; s)\mathcal{G}_k(q; s)\mathcal{T}_{ki}(q, p; s), \tag{2}$$

where s is the square of the total energy. p, p' and q stand respectively for the four-momenta of the initial, final and intermediate mesons in the center of mass (CM) frame. The indices i and f represent the initial and final meson channels, and k designates the intermediate state in the coupled-channel formalism. Since it is rather complicated to deal with the BS equation, we use its three-dimensional reduction, which is not unique. In the current work, we utilize the Blankenbecler-Sugar (BbS) equation [27, 28] that preserves the unitarity of two-body interaction for all energies and keeps Lorentz invariance. It is convenient to introduce the coupled-channel formalism and is expressed as

$$\mathcal{T}_{fi}(\mathbf{p}', \mathbf{p}; s) = \mathcal{V}_{fi}(\mathbf{p}', \mathbf{p}; s) + \frac{1}{(2\pi)^3}\int \frac{d^3q}{2E_{k1}(\mathbf{q})E_{k2}(\mathbf{q})}\mathcal{V}_{fk}(\mathbf{p}', \mathbf{q}; s)\frac{E_k(\mathbf{q})}{s - E_k^2(\mathbf{q})}\mathcal{T}_{ki}(\mathbf{q}, \mathbf{p}; s), \tag{3}$$

where $E_{ki} = (\mathbf{q}^2 + m_{ki})^{1/2}$ and $E_k = E_{k1} + E_{k2}$. The zeroth component of the momenta is determined by the propagator $\mathcal{G}_k$ given as $q_0 = (E_{k1} - E_{k2})/2$.

Since we are mainly interested in the a_1 meson, we need to consider only the two channels: $\pi\rho$ and $K\bar{K}^*$ ($\bar{K}K^*$) ones. Other channels such as the $\pi\omega$ and $\pi\phi$ do not contribute to the production of the a_1 meson. In the coupled-channel formalism, the kernel $\mathcal{V}_{fi}$ in Eq. (3) is expressed as

$$\mathcal{V}_{fi} = \begin{pmatrix} \mathcal{V}_{\pi\rho\to\pi\rho} & \mathcal{V}_{K\bar{K}^*\to\pi\rho} \\ \mathcal{V}_{\pi\rho\to K\bar{K}^*} & \mathcal{V}_{K\bar{K}^*\to K\bar{K}^*} \end{pmatrix}, \tag{4}$$

where the off-diagonal part of $\mathcal{V}_{fi}$ contains the transition from $\pi\rho \to K\bar{K}^*$ ($\bar{K}K^*$). Since K and K^* have no definite G-parity, we need to combine the $K\bar{K}^*$ and $\bar{K}K^*$ states, which gives a state with the definite G parity:

$$|K\bar{K}^*(\pm)\rangle = \frac{1}{\sqrt{2}}\left(|K\bar{K}^*\rangle \pm |\bar{K}K^*\rangle\right). \tag{5}$$

Note that we consider only the negative one because $\pi\rho$ has negative G-parity. We will see later that the $K\bar{K}^*$ channel with the positive G-parity decouples from the $\pi\rho$ channel.

The kernel $\mathcal{V}_{fi}$ in Eq. (4) is modeled by meson-exchange diagrams as drawn generically in Fig. 1. Since the a_1

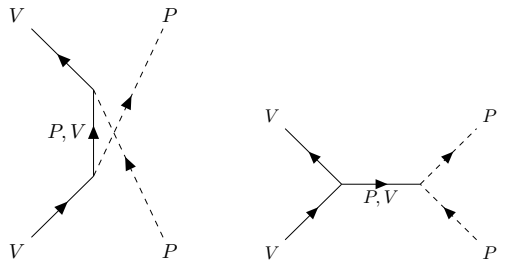


FIG. 1. The u- (left) and t-channels (right) of the meson-exchanged diagrams.

meson will be dynamically generated by the coupled-channel formalism, we do not include it in the s channel. The vertices in the Feynman diagrams are formulated from the SU(3) symmetric effective Lagrangians given by

$$\begin{aligned}
\mathcal{L}_{PPV} &= \sqrt{2}g_{PPV}\,\mathrm{Tr}\left([P, \partial_\mu P]\,V^\mu\right), \\
\mathcal{L}_{VVV} &= -\sqrt{2}g_{VVV}\,\mathrm{Tr}\left((\partial_\mu V_\nu - \partial_\nu V_\mu)V^\mu V^\nu\right), \\
\mathcal{L}_{PVV} &= \sqrt{2}\frac{g_{PVV}}{m_V}\,\varepsilon^{\mu\nu\alpha\beta}\mathrm{Tr}\left(\partial_\mu V_\nu \partial_\alpha V_\beta P\right),
\end{aligned} \tag{6}$$

where subscripts V and P denote the vector and pseudoscalar mesons involved in the vertices. m_V represents the mass of the vector meson. We choose $g_{PPV} = g_{VVV}$ by regarding the vector mesons as dynamical gauge bosons arising from hidden local gauge symmetry [25, 26]. The values of the coupling constants are taken from Ref. [24]: $g^2_{\pi\pi\rho}/4\pi = 2.84$ and $(g^2_{\pi\rho\omega}/4\pi)m^2_\omega = 7.5$. These couplings are related to the g_{PPV} and g_{PVV} by SU(3) symmetric factor as $g_{\pi\pi\rho} = 2g_{PPV}$ and $g_{\pi\rho\omega}m_\omega = 2g_{PVV}$. Since flavor SU(3) symmetry is broken, the coupling constants vary from the SU(3) symmetric case. When it is necessary, we change the values of the coupling constants, which are not far from the SU(3) symmetric ones, so that we can fit the experimental data. However, we regard the ϕ-exchange coupling constant as a free parameter. Its value we have selected differs from the SU(3) symmetric one by 1 %.

The trace operators in Eq. (6) run only over flavor space. The matrices for the pseudoscalar and vector mesons are expressed respectively as

$$P = \begin{pmatrix} \frac{1}{\sqrt{2}}\pi^0 + \frac{1}{\sqrt{6}}\eta & \pi^+ & K^+ \\ \pi^- & -\frac{1}{\sqrt{2}}\pi^0 + \frac{1}{\sqrt{6}}\eta & K^0 \\ K^- & \bar{K}^0 & -\frac{2}{\sqrt{6}}\eta \end{pmatrix}, \tag{7}$$

$$V_\mu = \begin{pmatrix} \frac{1}{\sqrt{2}}\rho^0_\mu + \frac{1}{\sqrt{2}}\omega_\mu & \rho^+_\mu & K^{*+}_\mu \\ \rho^-_\mu & -\frac{1}{\sqrt{2}}\rho^0_\mu + \frac{1}{\sqrt{2}}\omega_\mu & K^{*0}_\mu \\ K^{*-}_\mu & \bar{K}^{*0}_\mu & \phi_\mu, \end{pmatrix}. \tag{8}$$

where we employ the standard mixing for the ω_1 and ω_8 components such that the ω meson contains only the u and d quarks whereas the ϕ meson only comprises the strange quark. The mixing angle between η and η' is in the range between -10° and -20° [29]. It will only lead to $(2-6)$ % difference in the $g_{K\eta K^*}$ coupling constant, so that η' exchange will provide maximum 13 % of the η-exchange contribution to the $K\bar{K}^* \to K\bar{K}^*$ potential. Moreover, the contribution of η exchange to the potential is tiny. Therefore, for simplicity, we ignore η' meson exchange in the current study. The flavor part of Eq. (6) can be evaluated in the isospin bases and yield factors labeled as IS listed in the fourth column of Table I. Note that the IS factor contains both the SU(3) symmetric factor and isospin one.

TABLE I. The factor IS and cut-off Λ for all possible exchange diagram for each reaction. Note that the value inside the parentheses is given for the conjugate state of $K\bar{K}^*$ and m is the exchange mass.

Reaction	Exchange	Type	IS	$\Lambda - m$ [MeV]
$\pi\rho \to \pi\rho$	π	u	4	600
	ρ	t	-4	600
	ω	u	-4	600
$\pi\rho \to K\bar{K}^*(\bar{K}K^*)$	K	u	$-2(2)$	700
	K^*	t	$2(-2)$	750
$K\bar{K}^* \to K\bar{K}^*$	ρ	t	1	600
	ω	t	-1	600
	ϕ	t	-2	1400
$K\bar{K}^* \to \bar{K}K^*$	π	u	1	600
	η	u	-3	600
	ρ	u	-1	600
	ω	u	1	600
	ϕ	u	2	1400

From Table I, we find it obvious that the $K\bar{K}^*$ channel with positive G-parity cannot be coupled to the $\pi\rho$ channel.

Since the hadron has a finite size, we introduce the form factor at each vertex. We use the following parametrization for it

$$F(t) = \left(\frac{n\Lambda^2 - m^2}{n\Lambda^2 - t}\right)^n, \qquad F(u) = \left(\frac{n\Lambda^2 - m^2}{n\Lambda^2 - u}\right)^n, \tag{9}$$

where m denotes the mass of the exchange particle. n is determined by the power of the momentum in the vertex. For example, we take $n = 1$ for the VPP vertex whereas we choose $n = 2$ for the VVP one. Though the cut-off masses Λ are free parameters, we reduce the uncertainties by fixing their values as follows: we add $(600 - 700)$ MeV to the exchange mass. This idea is based on the fact that a heavier particle has a smaller size [30–32]. Thus, the value of Λ is also taken to be larger than that of the corresponding meson mass by around $(600 - 700)$ MeV. To fit the data, however, we choose a larger value of the cut-off mass especially for ϕ exchange, where its value is 1400 MeV higher than that of the exchanged meson mass. In addition, we drop out the energy and angular dependence of the form factors for the sake of simplicity [24].

We obtain the kernels $\mathcal{V}_{fi}$ by summing the amplitudes of all possible exchange diagrams listed in Table. I. There are only 3 possible diagrams that provide the Feynman amplitudes as functions of the Mandelstam variables and a type of exchanged mesons. The amplitudes for the t-channel with vector-meson exchange and for the u-channel with pseudoscalar-meson and vector-meson exchanges are respectively given by

$$\mathcal{A}_V^t(\mathbf{p}',\mathbf{p}) = \mathrm{IS}\, g_{PPV}^2\, F^2(t)\ (p_2+p_4)^\mu\ \left(g_{\mu\nu} - \frac{1}{m_V^2}(p_1-p_3)_\mu(p_1-p_3)_\nu\right)\mathcal{P}(t)$$
$$\times\left[(2p_1-p_3)\cdot\epsilon^*\epsilon^\nu + (2p_3-p_1)\cdot\epsilon\epsilon^{*\nu} - \epsilon\cdot\epsilon^*(p_1+p_3)^\nu\right], \tag{10}$$

$$\mathcal{A}_P^u(\mathbf{p}',\mathbf{p}) = -\mathrm{IS}\, g_{PPV}^2\, F^2(u)\ (2p_2-p_3)\cdot\epsilon^*\,\mathcal{P}(u)\ (2p_4-p_1)\cdot\epsilon, \tag{11}$$

$$\mathcal{A}_V^u(\mathbf{p}',\mathbf{p}) = -\mathrm{IS}\,\frac{g_{PVV}^2}{m_V^2}\, F^2(u)\,\varepsilon_{\mu\nu\alpha\beta}\,p_3^\mu\epsilon^{*\nu}(p_3-p_2)^\alpha\, g^{\beta\delta}\mathcal{P}(u)\,\varepsilon_{\gamma\sigma\eta\delta}p_1^\gamma\epsilon^\sigma(p_1-p_4)^\eta, \tag{12}$$

where $p_1(\mathbf{p})$ and $p_2(\mathbf{p})$ respectively denote the four momenta of the initial vector and pseudoscalar mesons whereas $p_3(\mathbf{p}')$ and $p_4(\mathbf{p}')$ are those of the final vector and pseudoscalar mesons respectively. The polarization vectors of the initial and final vector mesons are respectively labeled as $\epsilon(\mathbf{p})$ and $\epsilon^*(\mathbf{p}')$. As for the propagators of the exchange mesons, we utilize the static ones, following Ref. [24].

Since the a_1 meson arises from the S-wave transition amplitude, we carry out the partial wave decomposition of the kernel and transition amplitudes. The partial-wave helicity amplitudes can be obtained by projecting the amplitudes onto the total angular momentum J

$$\mathcal{T}^{J(fi)}_{\lambda'\lambda}(\mathrm{p}',\mathrm{p}) = \mathcal{V}^{J(fi)}_{\lambda'\lambda}(\mathrm{p}',\mathrm{p}) + \frac{1}{(2\pi)^3}\sum_{k,\lambda_k}\int\frac{\mathrm{q}^2 d\mathrm{q}}{2E_{k1}(\mathrm{q})E_{k2}(\mathrm{q})}\mathcal{V}^{J(fk)}_{\lambda'\lambda_k}(\mathrm{p}',\mathrm{q})\frac{E_k(\mathrm{q})}{s-E_k^2(\mathrm{q})}\mathcal{T}^{J(ki)}_{\lambda_k\lambda}(\mathrm{q},\mathrm{p}), \tag{13}$$

where λ', λ, and λ_k denote the helicities of the final (f), initial (i) and intermediate (k) states, respectively. The partial-wave kernel amplitudes can be expressed as

$$\mathcal{V}^{J(fi)}_{\lambda'\lambda}(\mathrm{p}',\mathrm{p}) = 2\pi\int d(\cos\theta)\, d^J_{\lambda'\lambda}(\theta)\,\mathcal{V}^{fi}_{\lambda'\lambda}(\mathrm{p}',\mathrm{p},\theta), \tag{14}$$

where θ denotes the scattering angle and $d^J_{\lambda'\lambda}(\theta)$ stand for the matrix elements of the Wigner D functions. The partial-wave $\mathcal{T}$ amplitude is also expressed in a similar manner.

The partial-wave coupled integral equation in Eq. (13) is solved numerically after we regularize the singularity arising from the two-body meson propagator $\mathcal{G}$. We build the matrix $\mathcal{V}$ in momentum space, including both the $\pi\rho$ and $K\bar{K}^*$ channels. Then $\mathcal{T}$ matrix can be derived by the Haftel-Tabakin's method of the matrix inversion [33]

$$\mathcal{T} = \left(1-\mathcal{V}\tilde{\mathcal{G}}\right)^{-1}\mathcal{V}. \tag{15}$$

It is convenient to write the $\mathcal{T}$ matrix in the particle basis [34]. Thus, we define $\mathcal{T}_{IJL}$ as the $\mathcal{T}$ matrix for a given total isospin I, total angular momentum J, and orbital angular momentum L.

III. a_1 MESON AS A $K\bar{K}^*$ MOLECULAR STATE

We discuss now how the a_1 meson can be dynamically generated by the coupled channel formalism. In Fig. 2, we draw the real part of $\mathcal{T}_{110}$ in the $K\bar{K}^* \to K\bar{K}^*$ channel, which corresponds to the quantum numbers of the a_1 resonance. Here we will only consider the $K\bar{K}^*$ single channel to examine how the resonance behavior arises from the integral equation. The kernel amplitude $\mathcal{V}_{K\bar{K}^*\to K\bar{K}^*}$ itself does not show any resonance behavior, which is depicted as the dashed line. On the other hand, the full transition amplitude generates the singularity below the $K\bar{K}^*$ threshold energy after the integral equation is solved. The pole is positioned on the real energy axis. This singularity occurs from the strong attraction of the t-channel exchange. Specifically, this attractive potential comes from the ϕ exchange diagram since the ρ and ω contribution cancelled each other as we can see from their IS factor. This singular behavior in $\mathcal{T}$ is responsible for creating the a_1 meson in the $\pi\rho \to \pi\rho$ reaction. The remarkable point is that it only appears below the $K\bar{K}^*$ threshold. Once we introduce the $\pi\rho$ channel and make it coupled to the $K\bar{K}^*$ one, the pole moves to the second Riemann sheet in the complex energy plane. This indicates that the finite width of the a_1 resonance is caused by the coupling of the $K\bar{K}^*$ channel with the $\pi\rho$ one.

To compared the experimental data [7] given in an arbitrary unit, one can take the total cross section to be

$$\sigma \equiv \sigma_{\pi\rho}\left(t=m_\rho^2, M_{\pi\rho}\right) = -C\,\mathrm{Im}[\mathcal{T}_{\pi\rho}(M_{\pi\rho})], \tag{16}$$

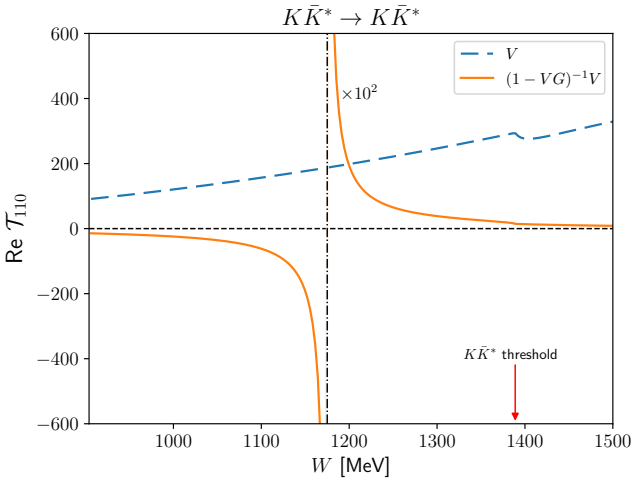


FIG. 2. Real part of $\mathcal{T}_{110}$ in the $K\bar{K}^* \to K\bar{K}^*$ reaction as a function of energy. Here we label the kernel amplitude $\mathcal{V}_{K\bar{K}^*\to K\bar{K}^*}$ as $\mathcal{V}$. The dashed line depicts $\mathcal{V}$, whereas the solid curve draws $(1-\mathcal{V}\mathcal{G})^{-1}\mathcal{V}$.

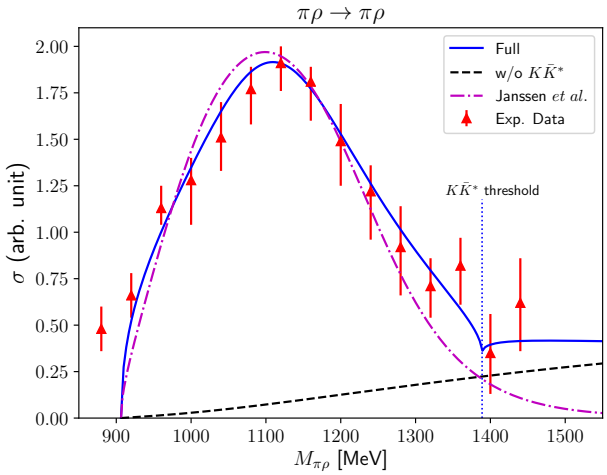


FIG. 3. Comparison of the $\pi\rho \to \pi\rho$ total cross section for $IJL = 110$ as a function of $\pi\rho$ invariant mass with that from Ref. [24]. The solid curve draws the result from the present work whereas the dot-dashed one depicts that from Ref. [24]. The dashed line exhibits the result with the $K\bar{K}^*$ channel turned off. The experimental data are taken from Ref. [7].

where C is the constant to match the data to the results from a theoretical model. The full transition amplitude $\mathcal{T}_{\pi\rho}$ is obtained by solving the integral equation in the coupled-channel formalism, given in Eq. (3). Figure 3 shows the result for σ as a function of the $\pi\rho$ invariant mass. The solid curve draws the current result whereas the dot-dashed one corresponds to that from Ref. [24] in which the a_1 meson was explicitly introduced as a s-channel pole diagram with the $\pi\rho$ channel only considered. The result from Ref. [24] shows a symmetric shape, since the a_1 pole diagram governs it. On the other hand, the present result reveals a dynamical feature of the a_1 resonance. The physical a_1 meson is generated only by coupling the $\pi\rho$ channel with the $K\bar{K}^*$ one. It describes well the experimental data on $\pi\rho$ scattering near the $\pi\rho$ threshold. The S-wave total cross section rapidly increases and reaches the maximum value at around 1 100 MeV. While the result from Ref. [24] falls off rapidly, so that it is underestimated in the vicinity of the $K\bar{K}^*$ threshold, the present result decreases less rapidly. It explains well the data even near the $K\bar{K}^*$ threshold. If we turn off the $K\bar{K}^*$ channel, the result cannot yield the $a_1(1260)$ resonance structure at all. Thus, the $K\bar{K}^*$ channel plays a critical role in generating the a_1 resonance. A similar situation can be found in the case of the $f_0(980)$ meson. In Ref. [19], $\pi\pi$ scattering was investigated within the meson-exchange model, where the $f_0(980)$ resonance can only appear when the $K\bar{K}$ channel was included. A similar feature was also observed in Ref. [23]. So, the $f_0(980)$ meson is often considered as a $K\bar{K}$ molecular state. Similarly, the $a_1(1260)$ resonance can be called a $K\bar{K}^*$ molecular state.

To scrutinize the $a_1(1260)$ resonance based on the current work, we evaluate the pole position for this resonance in

the second Riemann sheet and coupling strength at the pole position. We utilize the analytic continuation method [35] to determine the scattering matrix on the complex energy plane of total energy. We locate the pole position a_1 at $\sqrt{s_R} = (1170.7 - i173.0)$ MeV in the complex energy plane. Since there is no other resonance nearby, we can determine clearly its position. From the pole position we found that the width of the a_1 meson is in agreement with that from Ref. [7], where $\Gamma = (380 \pm 100)$ MeV was obtained by using the Bowler model fit. Experimentally, the width of the $a_1(1260)$ meson is given in the wide range: $\Gamma_{a_1} = (250 - 600)$ MeV [29]. The present work provides almost the center value of $\Gamma_{a_1} \approx 350$ MeV, compared to the PDG data.

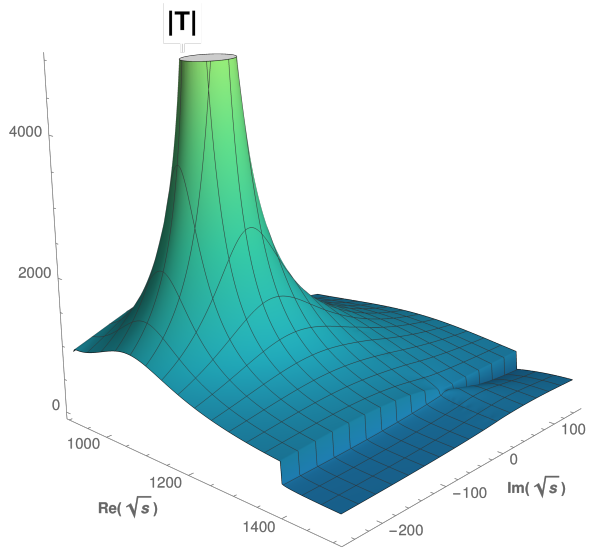


FIG. 4. The 3D plot of absolute T matrix as a function of complex energy.

To see the a_1 resonance structure more explicitly, we also present the 3D plot of the $|T|$ in the complex energy plane, as illustrated in Fig. 4. To derive the coupling strengths of the a_1 meson coupled to the $\pi\rho$ and $K\bar{K}^*$ channels, we derive it from the residue of the transition amplitude defined as $\mathcal{R}_{a,b}$:

$$\mathcal{R}_{a,b} = \lim_{s \to s_R} (s - s_R)\, \mathcal{T}_{a,b}/4\pi. \tag{17}$$

We divide the partial-wave component of the T-matrix with the factor 4π since we use different definition of partial wave expansion in Eq. (14). The coupling strengths are defined as the square root of the residue of the transition amplitude, so that we obtain them as

$$g^{a_1}_{\pi\rho} = \sqrt{\mathcal{R}^{a_1}_{\pi\rho,\pi\rho}} = (5.75 - i1.35)\,[\text{GeV}], \tag{18}$$

$$g^{a_1}_{K\bar{K}^*} = \sqrt{\mathcal{R}^{a_1}_{K\bar{K}^*,K\bar{K}^*}} = (12.37 - i2.31)\,[\text{GeV}]. \tag{19}$$

Note that we choose the positive signs for both coupling strengths, since we are not able to determine them.

Finally but not least, we want briefly to mention about the compositeness of the a_1 meson. Weinberg shows the possibility to quantify the nature of the bound state through the renormalization constant [36]. It is possible to extend this idea to the virtual and resonance state. In Ref. [37], for instance, the compositeness of an unstable resonance was studied by examining the coupling strength and the derivative of a two-body loop propagator evaluated in the second Riemann sheet where the resonance's pole is located. In Ref. [38] the positive definite compositeness of the resonance was studied. However, it is valid to examine the compositeness only when the threshold energy is less than the mass of a resonance. Therefore, it is rather complicated to calculate the compositeness to prove that K and K^* dominate in the a_1 since the $K\bar{K}^*$ threshold energy is larger than the a_1 mass in the present work.

IV. SUMMARY AND CONCLUSIONS

In the present work, we studied $\pi\rho$ scattering based on the meson-exchange model, focusing on the $a_1(1260)$ resonance appearing in the S-wave total cross section. We showed that the coupled-channel formalism including the

$\pi\rho$ and $K\bar{K}^*$ channels generated the a_1 meson dynamically. The $K\bar{K}^*$ channel plays an essential role in producing the a_1 meson. We solved the integral equation for $K\bar{K}^*$ scattering and found a pole on the real energy axis. Once we introduced the $\pi\rho$ channel and coupled it to the $K\bar{K}^*$ channel, we observed that the a_1 resonance arises dynamically in $\pi\rho$ scattering. We obtained the pole position of the a_1 resonance at $\sqrt{s_R} = (1170.7 - i173.0)$ MeV. The present result is much better than the one in the previous study, where the a_1 meson was introduced explicitly in the s-channel pole diagram with the $\pi\rho$ single channel considered only. We also derived the coupling strengths $g^{a_1}_{\pi\rho}$ and $g^{a_1}_{K\bar{K}^*}$ from the residue of the transition amplitude. These results imply that the dynamically generated a_1 meson may be interpreted as a $K\bar{K}^*$ molecular state.

ACKNOWLEDGMENTS

The present work was supported by Basic Science Research Program through the National Research Foundation of Korea funded by the Korean government (Ministry of Education, Science and Technology, MEST), Grant-No. 2021R1A2C2093368 and 2018R1A5A1025563.

[1] S. Weinberg, Precise relations between the spectra of vector and axial vector mesons, Phys. Rev. Lett. **18**, 507 (1967).
[2] M. Gell-Mann and M. Levy, The axial vector current in beta decay, Nuovo Cim. **16**, 705 (1960).
[3] C. Daum *et al.* (ACCMOR), Experimental proof of the existence of the A1 meson, Phys. Lett. B **89**, 281 (1980).
[4] H. Albrecht *et al.* (ARGUS), Measurement of tau decays Into three charged pions, Z. Phys. C **33**, 7 (1986).
[5] D. M. Asner *et al.* (CLEO), Hadronic structure in the decay $\tau \to \nu_\tau \pi^- \pi^0 \pi^0$ and the sign of the tau-neutrino helicity, Phys. Rev. D **61**, 012002 (2000), arXiv:hep-ex/9902022.
[6] R. Aaij *et al.* (LHCb), Studies of the resonance structure in $D^0 \to K^\mp \pi^\pm \pi^\pm \pi^\mp$ decays, Eur. Phys. J. C **78**, 443 (2018), arXiv:1712.08609 [hep-ex].
[7] J. A. Dankowych *et al.*, Evidence for $I = 1(A1)$ and $I = 0(H)$ axial vector resonances in charge exchange, Phys. Rev. Lett. **46**, 580 (1981).
[8] A. Drutskoy *et al.* (Belle), Observation of $B \to D^* K^- K^{0*}$ decays, Phys. Lett. B **542**, 171 (2002), arXiv:hep-ex/0207041.
[9] T. E. Coan *et al.* (CLEO), Wess-Zumino current and the structure of the decay $\tau \to K^- K^+ \pi^- \nu_\tau$, Phys. Rev. Lett. **92**, 232001 (2004), arXiv:hep-ex/0401005.
[10] J. L. Basdevant and E. L. Berger, Unitary coupled-channel analysis of diffractive production of the a_1 resonance, Phys. Rev. D **16**, 657 (1977).
[11] L. Roca, E. Oset, and J. Singh, Low lying axial-vector mesons as dynamically generated resonances, Phys. Rev. D **72**, 014002 (2005), arXiv:hep-ph/0503273.
[12] M. F. M. Lutz and E. E. Kolomeitsev, On meson resonances and chiral symmetry, Nucl. Phys. A **730**, 392 (2004), arXiv:nucl-th/0307039.
[13] H. Nagahiro, K. Nawa, S. Ozaki, D. Jido, and A. Hosaka, Composite and elementary natures of $a_1(1260)$ meson, Phys. Rev. D **83**, 111504 (2011), arXiv:1101.3623 [hep-ph].
[14] R. L. Jaffe, Multi-quark Hadrons. 1. The phenomenology of (2 quark 2 anti-quark) mesons, Phys. Rev. D **15**, 267 (1977).
[15] N. N. Achasov, S. A. Devyanin, and G. N. Shestakov, Is There a 'Signature' of the δ (980) meson four quark nature?, Phys. Lett. B **96**, 168 (1980).
[16] V. Baru, J. Haidenbauer, C. Hanhart, Y. Kalashnikova, and A. E. Kudryavtsev, Evidence that the $a_0(980)$ and $f_0(980)$ are not elementary particles, Phys. Lett. B **586**, 53 (2004), arXiv:hep-ph/0308129.
[17] Z.-Q. Wang, X.-W. Kang, J. A. Oller, and L. Zhang, Analysis on the composite nature of the light scalar mesons f0(980) and a0(980), Phys. Rev. D **105**, 074016 (2022), arXiv:2201.00492 [hep-ph].
[18] D. Lohse, J. W. Durso, K. Holinde, and J. Speth, Scalar Mesons in $\pi\pi$ and $K\pi$ Scattering, Phys. Lett. B **234**, 235 (1990).
[19] D. Lohse, J. W. Durso, K. Holinde, and J. Speth, Meson exchange model for pseudoscalar meson meson scattering, Nucl. Phys. A **516**, 513 (1990).
[20] C. Amsler and N. A. Tornqvist, Mesons beyond the naive quark model, Phys. Rept. **389**, 61 (2004).
[21] H. A. Ahmed and C. W. Xiao, Study the molecular nature of σ, $f_0(980)$, and $a_0(980)$ states, Phys. Rev. D **101**, 094034 (2020), arXiv:2001.08141 [hep-ph].
[22] N. N. Achasov, J. V. Bennett, A. V. Kiselev, E. A. Kozyrev, and G. N. Shestakov, Evidence of the four-quark nature of $f_0(980)$ and $f_0(500)$, Phys. Rev. D **103**, 014010 (2021), arXiv:2009.04191 [hep-ph].
[23] J. A. Oller and E. Oset, Chiral symmetry amplitudes in the S wave isoscalar and isovector channels and the σ, $f_0(980)$, $a_0(980)$ scalar mesons, Nucl. Phys. A **620**, 438 (1997), [Erratum: Nucl.Phys.A 652, 407–409 (1999)], arXiv:hep-ph/9702314.
[24] G. Janssen, K. Holinde, and J. Speth, A meson exchange model for π ρ scattering, Phys. Rev. C **49**, 2763 (1994).
[25] M. Bando, T. Kugo, S. Uehara, K. Yamawaki, and T. Yanagida, Is rho meson a dynamical gauge boson of hidden local symmetry?, Phys. Rev. Lett. **54**, 1215 (1985).

[26] M. Bando, T. Kugo, and K. Yamawaki, On the vector mesons as dynamical gauge bosons of hidden local symmetries, Nucl. Phys. B **259**, 493 (1985).
[27] R. Blankenbecler and R. Sugar, Linear integral equations for relativistic multichannel scattering, Phys. Rev. **142**, 1051 (1966).
[28] R. Aaron, R. D. Amado, and J. E. Young, Relativistic three-body theory with applications to $\pi^- n$ scattering, Phys. Rev. **174**, 2022 (1968).
[29] R. L. W. et al. (Particle Data Group), The Review of Particle Physics (2022), Prog. Theor. Exp. Phys. **2022**, 083C01 (2022).
[30] J.-Y. Kim and H.-C. Kim, Electromagnetic form factors of singly heavy baryons in the self-consistent SU(3) chiral quark-soliton model, Phys. Rev. D **97**, 114009 (2018), arXiv:1803.04069 [hep-ph].
[31] J.-Y. Kim, H.-C. Kim, G.-S. Yang, and M. Oka, Electromagnetic transitions of the singly charmed baryons with spin 3/2, Phys. Rev. D **103**, 074025 (2021), arXiv:2101.10653 [hep-ph].
[32] H.-Y. Won, J.-Y. Kim, and H.-C. Kim, Gravitational form factors of the baryon octet with flavor SU(3) symmetry breaking, (2022), arXiv:2210.03320 [hep-ph].
[33] M. I. Haftel and F. Tabakin, Nuclear saturation and the smoothness of nucleon-nucleon potentials, Nucl. Phys. A **158**, 1 (1970).
[34] R. Machleidt, K. Holinde, and C. Elster, The Bonn meson exchange model for the nucleon nucleon Interaction, Phys. Rept. **149**, 1 (1987).
[35] N. Suzuki, T. Sato, and T. S. H. Lee, Extraction of Resonances from Meson-Nucleon Reactions, Phys. Rev. C **79**, 025205 (2009), arXiv:0806.2043 [nucl-th].
[36] S. Weinberg, Elementary particle theory of composite particles, Phys. Rev. **130**, 776 (1963).
[37] T. Hyodo, Structure and compositeness of hadron resonances, Int. J. Mod. Phys. A **28**, 1330045 (2013), arXiv:1310.1176 [hep-ph].
[38] Z.-H. Guo and J. A. Oller, Probabilistic interpretation of compositeness relation for resonances, Phys. Rev. D **93**, 096001 (2016), arXiv:1508.06400 [hep-ph].